J|A|C|S
ARTICLES
Published on Web 02/24/2006

Electrodeposition of Au Monolayer on Pt(111) Mediated by Self-Assembled Monolayers

Yaw-Chia Yang,[†] Shueh-Lin Yau,[‡] and Yuh-Lang Lee*,[†]

Contribution from the Department of Chemical Engineering, National Cheng Kung University, Tainan 70101, Taiwan and CREST, JST, 4-1-8 Kawaguchi, Saitama 332-0012, Japan

Received October 11, 2005; E-mail: yllee@mail.ncku.edu.tw

Abstract: In-situ scanning tunneling microscopy (STM), cyclic voltammetry (CV), and infrared reflection-adsorption spectroscopy (IRRAS) have been used to examine the electrodeposition of gold onto Pt(111) electrodes modified with benzenethiol (BT) and benzene-1,2-dithiol (BDT) in 0.1 M $HClO_4$ containing 10 μM $HAuCl_4$. Both BT and BDT were attached to Pt(111) via one sulfur headgroup. STM and IRRAS results indicated that the other SH group of BDT was pendant in the electrolyte. Both BT and BDT formed (2×2) structures at the coverage of 0.25, and they were transformed into ($\sqrt{3} \times \sqrt{3}$)$R30°$ as the coverage was raised to 0.33. These two organic surface modifiers resulted in 3D and 2D gold islands at BT- and BDT-coated Pt(111) electrodes, respectively. The pendant SH group of BDT could interact specifically with gold adspecies to immobilize gold adatoms on the Pt(111) substrate, which yields a 2D growth of gold deposition. Molecular resolution STM revealed an ordered array of ($6 \times 2\sqrt{13}$) after a full monolayer of gold was plated on the BDT/Pt(111) electrode. Since BDT was strongly adsorbed on Pt(111), gold adatoms only occupied free sites between BDT admolecules on Pt(111). This is supported by a stripping voltammetric analysis, which reveals no reductive desorption of BDT admolecules at a gold-deposited BDT/Pt(111) electrode. It seems that the BDT adlayer acted as the template for gold deposit on Pt(111). In contrast, a BT adlayer yielded 3D gold deposit on Pt(111). This study demonstrates unambiguously that organic surface modifiers could contribute greatly to the electrodeposition of metal adatoms.

1. Introduction

The deposition of heterogeneous metallic thin films has been of great interest in the disciplines of surface physics and material science. Rigorous experimental efforts have yielded insights into the growth kinetics and conditions needed to facilitate epitaxial growth of thin films in a vacuum.[1] Meanwhile, organic additives, known as "leveling agent" or "brightener", are frequently added in the electrodeposition baths to produce smooth metallic thin films. Unfortunately, even with the advances in surface probing techniques, the role of organic additives in electrodeposition remains elusive and finding the conditions needed for generating smooth metallic thin films has been mostly empirical.[2,3]

The growth mode of heterogeneous thin films has been shown to depend primarily on the adsorbate−substrate interaction. A few electrochemical systems including Ni/Au(111), Cu/Au(100), and Cu/Ag(100) were found to follow the layer-by-layer growth mode for the first several monolayers.[4−6] For systems which are not thermodynamically favorable to proceed in the layered mode, several strategies were developed for both heteroepitaxial and homoepitaxial systems. For example, artificial sites created using argon ion bombardment can induce homoepitaxy of Ag on Ag(111).[7] Alternatively, a monolayer or submonolayer of foreign atoms, known as "surfactants", can enhance nucleation rates or/and reduce activation barriers for adatoms to diffuse across steps.[8−11] A layer-by-layer growth mode results. For example, Pb- or Cu-mediated deposition of silver on Au(111) is used to illustrate the surfactant-induced epitaxy where Pb or Cu adatoms enhance nucleation and coalescence of 2D Ag islands.[12]

Self-assembled monolayers (SAMs) are shown to modify metal deposition in both a vacuum[13−20] and electrochemistry.[20−26]

[†] National Cheng Kung University.
[‡] CREST.

(1) Zhang, Z.; Lagally, M. G. *Science* **1997**, *276*, 377−383.
(2) Nichols, R. J.; Beckmann, W.; Meyer, H.; Batina, N.; Kolb, D. M. *J. Electroanal. Chem.* **1992**, *330*, 381.
(3) Plieth, W. *Electrochim. Acta* **1992**, *37*, 2115.
(4) Magnussen, O. M.; Moller, F. A.; Lachenwitzer, A.; Behm, R. J. In *Electrochemical Synthesis and Modification of Materials*; Materials Research Society Symposium, Boston, MA, Dec 2−5, 1996; Andricacos, P. C., Corcoran, S. G., Delplancke, J. L., Moffat, T. P., Searson, P. C., Eds.; Materials Research Society: Pittsburgh, PA, 1997; Vol. 451, pp 43−48.
(5) Kolb, D. M.; Randler, R. J.; Wielgosz, R. I.; Ziegler, J. C. Materials Research Society Symposium, Boston, MA, Dec 2−5, 1996; Andricacos, P. C., Corcoran, S. G., Delplancke, J. L., Moffat, T. P., Searson, P. C., Eds.; Materials Research Society: Pittsburgh, PA, 1997; Vol. 451, pp 19−30.
(6) Dietterle, M.; Will, T.; Kolb, D. M. *Surf. Sci.* **1998**, *396*, 189−197.
(7) Rosenfeld, G.; Servaty, R.; Teichert, C.; Poelsema, B.; Comsa, G. *Phys. Rev. Lett.* **1993**, *71*, 895−898.
(8) van der Vegt, H. A.; van Pinxteren, H. M.; Lohmeier, M.; Vlieg, E.; Thornton, J. M. C. *Phys. Rev. Lett.* **1992**, *68*, 3335−3338.
(9) Zhang, Z.; Lagally, M. G. *Phys. Rev. Lett.* **1994**, *72*, 693−696.
(10) Meyer, J. A.; Vrijmoeth, J.; van der Vegt, H. A.; Vlieg, E.; Behm, R. J. *Phys. Rev. B* **1995**, *51*, 14790−14793.
(11) Harris, S. *Phys. Rev. B* **1995**, *52*, 16793−16795.
(12) Sieradzki, K.; Brankovic, S. R.; Dimitrov, N. *Science* **1999**, *284*, 138−141.
(13) Herdt, G. C.; Jung, D. R.; Czanderna, A. W. *Prog. Surf. Sci.* **1995**, *50*, 103−129.
(14) Tarlov, M. J. *Langmuir* **1992**, *8*, 80−89.
(15) Czanderna, A. W.; King, D. E.; Spaulding, D. *J. Vac. Sci. Technol. A* **1991**, *9*, 2607−2613.

Studies have addressed how metal adatoms interact with the functional groups of SAMs and how metal adatoms are transported on substrate and diffuse into a SAM adlayer.[13−20] Comparatively, the need for having charge exchange between the electrode and adatoms and shedding the coordinated moieties of metal complexes complicates electrochemical deposition (ECD). The presence of organic additives complicates the situation further. Studies have been conducted to elucidate the effects of adsorbed alkanethiols on ECD.[22−23,27] Long-chain alkanethiols on Au(111) can inhibit completely or partially Cu deposition, depending on the chain length of the admolecules.[22,23] Thiophenol molecule, which is reported to exhibit higher charge permeability, still inhibits Cu deposition.[20,27,28]

Kinetic models and physical arguments developed for epitaxial deposition indicate that 2D growth of metallic thin films lies in the high nucleation rate, high diffusion rate of adatoms on top of the deposited islands and down a descending step. High adhesion of adatoms to substrate can afford a 2D growth mode. Now a thiol admolecule, attached to an electrode with its sulfur headgroup, can interact with the deposited metal via its organic end group to yield a 2D growth mode. The present study illustrates this idea using benzene-1,2-dithiol (BDT) as the mediator for gold deposition on Pt(111). The use of Pt as the substrate greatly simplifies the study because thiol molecules such as benzenethiol and hexanethiol are adsorbed in long-range ordered adlattices nearly without pinhole, as observed consistently on thiol-modified Pt(111).[29] In the present study we employed STM to examine the adsorption of BDT on Pt(111) and gold deposition on BT- and BDT-coated Pt(111) electrode. We show that gold deposition on these two electrodes proceeded in distinctly different modes, which is associated with different chemical structures.

2. Experimental Section

A platinum single-crystal bead was obtained by melting the end of a Pt wire according to a procedure described previously.[30−32] The Pt electrode was annealed with a hydrogen flame, followed by rapid quenching in Millipore water. The thermal oxide layer produced by the annealing process was reduced electrochemically; a potential of 0.05 V was applied for 10 min in 0.1 M $HClO_4$ prior to addition of BT and BDT. The surface state of the Pt electrode was diagnosed with cyclic voltammetry and STM imaging.

Triple-distilled Millipore water was used to prepare all solutions used in this study. Ultrapure perchloric acid was purchased from Merck Inc. (Darmstadt, Germany). Benzenethiol (98% purity) and benzene-1,2-dithiol (95% purity) were supplied by Merck Inc. and Fluka, respectively. Hydrogen tetrachloroaurate(III) ($HAuCl_4 \cdot 3H_2O$) of 99.99% purity was purchased from Alfa Aesar (Ward Hill, MA). All chemicals were used as received without further purification.

The scanning tunneling microscope (STM) was a Nanoscope-E (Santa Barbara, CA), and the tip was prepared by electrochemical etching of tungsten wire (0.25 mm in diameter) in 2 M KOH. The tip was further painted with nail polish for insulation, and the leakage current of the tip at the open-circuit potential was less than 0.05 nA. The in-situ STM imaging was operated at the constant-current mode. A reversible hydrogen electrode (RHE) was used as the reference electrode in electrochemical and STM measurements. All potentials described here are referred to a RHE scale.

The SAMs were prepared and in-situ imaged in 0.1 M $HClO_4$ solution containing about 100 μM BDT (or BT). Typically, the potential of the Pt(111) electrode was held at 0.15 V, which is in the potential region (between 0.05 and 0.3 V) for ordered molecular adlattices. After an ordered structure of SAM was accomplished, the solution containing the organosulfur was replaced by 0.1 M $HClO_4$ solution and the Au deposition performed after dosing 0.01 mM $HAuCl_4$.

Infrared reflection-adsorption spectroscopy (IRRAS) was used to characterize the configurations of BT and BDT on Pt(111) surface. The Fourier transform IR spectrometer was made with a Perkin-Elmer Spectrum GX equipped with a liquid nitrogen cooled MCT detector and operated at a spectral resolution of 8 cm^{-1}. The unpolarized IR beam was incident at 80° with respect to the surface normal of Pt surface. A Pt(111) single-crystal disk (7.8 mm in diameter, 2 mm in thickness) was used in this experiment for obtaining a large (111) surface available for this measurement. The cleaned Pt disk was first used to get the background signal (termed as I_0). The following assembly process of BDT or BT was performed in the same electrochemical system as that for STM imaging. The SAM-modified Pt(111) surface was then analyzed, and the intensity is termed I. The spectra are presented in the absorbance units defined as $-\log(I/I_0)$.

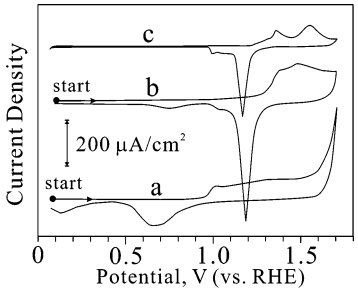

Figure 1. Cyclic voltammograms recorded at 50 mV/s with (a) BDT/Pt(111), (b) gold-plated BDT/Pt(111), and (c) Au(111) electrodes in 0.1 M $HClO_4$. BDT was adsorbed at 0.1 V. Gold was deposited on BDT-modified Pt(111) at 0.1 V for 10 min in 0.1 M $HClO_4$ + 0.01 mM $HAuCl_4$.

3. Results and Discussion

Cyclic Voltammetry. Figure 1 shows the cyclic voltammograms (CVs) recorded at 50 mV/s with (a) BDT/Pt(111) and (b) gold-plated BDT/Pt(111) electrodes in 0.1 M $HClO_4$. BDT was adsorbed from a 0.1 M $HClO_4$ solution containing 100 μM BDT at 0.1 V. The excursion of potential from 0.1 to 1.7 V resulted in a featureless $i-V$ profile between 0.1 and 0.9 V,

(16) Herdt, G. C.; Czanderna, A. W. *Surf. Sci. Lett.* **1993**, *297*, L109−L112.
(17) Fisher, G. L.; Walker, A. V.; Hooper, A. E.; Tighe, T. B.; Bahnck, K. B.; Skriba, H. T.; Reinard, M. D.; Haynie, B. C.; Opila, R. L.; Winograd, N.; Allara, D. L. *J. Am. Chem. Soc.* **2002**, *124*, 5528−5542.
(18) Walker, A. V.; Tighe, T. B.; Cabarcos, O. M.; Reinard, M. D.; Haynie, B. C.; Uppili, S.; Winograd, N.; Allara, D. L. *J. Am. Chem. Soc.* **2004**, *126*, 3954−3963.
(19) Colavita, P. E.; Doescher, M. S.; Molliet, A.; Evans, U.; Reddic, J.; Zhou, J.; Chen, D.; Miney, P. G.; Myrick, M. L. *Langmuir* **2002**, *18*, 8503−8509.
(20) Doescher, M. S.; Tour, J. M.; Rawlett, A. M.; Myrick, M. L. *J. Phys. Chem. B* **2001**, *105*, 105−110.
(21) Sondag Huethorst, J. A. M.; Fokkink, L. G. J. *Langmuir* **1995**, *11*, 2237−2241.
(22) Whelan, C. M.; Smyth, M. R.; Barnes, C. J. *J. Electroanal. Chem.* **1998**, *441*, 109−129.
(23) Nishizawa, M.; Sunagawa, T.; Yoneyama, H. *Langmuir* **1997**, *13*, 5215−5217.
(24) Gilbert, S. E.; Cavalleri, O.; Kern, K. *J. Phys. Chem.* **1996**, *100*, 12123−12130.
(25) Cavalleri, O.; Gilbert, S. E.; Kern, K. *Chem. Phys. Lett.* **1997**, *269*, 479−484.
(26) Oyamatsu, D.; Nishizawa, M.; Kuwabata, S.; Yoneyama, H. *Langmuir* **1998**, *14*, 3298−3302.
(27) Schneeweiss, M. A.; Hagenström, H.; Esplandiu, M. J.; Kolb, D. M. *Appl. Phys. A* **1999**, *69*, 537−551.
(28) Whelan, C. M.; Smyth, M. R.; Barnes, C. J. *Langmuir* **1999**, *15*, 116−126.
(29) Yang, Y. C.; Yen, Y. P.; Ou Yang, L. Y.; Yau, S. L.; Itaya, K. *Langmuir* **2004**, *20*, 10030−10037.
(30) Wu, Z. L.; Zang, Z. H.; Yau, S. L. *Langmuir* **2000**, *16*, 3522−3528.
(31) Wan, L. J.; Yau, S. L.; Itaya, K. *J. Phys. Chem.* **1995**, *99*, 9507−9513.
(32) Clavilier, J.; Rodes, A.; El Achi, K.; Zamakhchari, M. A. *J. Chem. Phys.* **1991**, *88*, 1291.

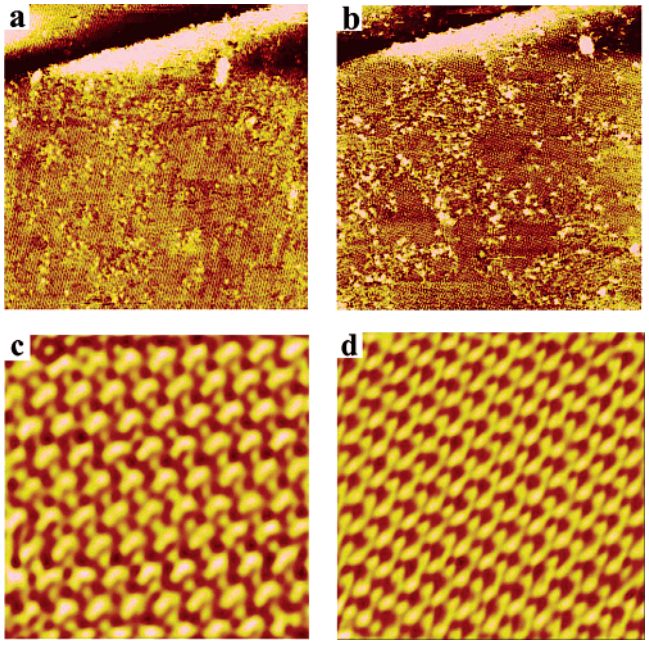

Figure 2. In-situ constant-current STM images obtained with Pt(111) immersed in 0.1 M $HClO_4$ + 100 μM BDT. STM scanning at the same area at 45 and 85 min after BDT was added resulted in two gross scans in a and b. The high-resolution scans in c and d highlight molecular structures in a and b, respectively.

which confirmed the adsorption of BDT on the Pt(111) electrode. Both the BT and BDT monolayers were stable toward extensive potential cycling between 0.05 and 0.9 V. The gradual rise in current density at $E > 0.9$ V is associated with the oxidation of BDT admolecules, whereas oxidation of Pt electrode did not occur until 1.7 V, as indicated by the reduction of oxide at 0.65 V in the following negative scan.

To elucidate the state of a gold-plated BDT/Pt(111) electrode, we obtained a CV after gold was deposited potentiostatically at 0.1 V for 10 min in 0.1 M $HClO_4$ + 0.01 mM $HAuCl_4$. The solution was replaced with 0.1 M $HClO_4$, followed by ramping positively from 0.05 to 1.7 V at a scan rate of 50 mV/s. The resultant CV profile shown in Figure 1b is featureless between 0.05 and 1.2 V, while broad peaks were observed between 1.2 and 1.7 V, attributed mainly to oxidation of gold. This CV result is comparable to that obtained with an Au(111) electrode (Figure 1c) except that of Au(111) exhibits better defined oxidation features at $E > 1.2$ V.

In-situ STM of Pt(111) Modified with Benzene-1,2-dithiol. Shown in Figure 2 are STM results obtained with Pt(111) modified with BDT at 0.15 V in 0.1 M $HClO_4$. The imaging conditions were 200 mV and 3 nA. It is emphasized that the hexagonal lattice with an interatomic spacing of 2.8 Å ascribed to the Pt(111) electrode was first discerned by high-resolution STM scans prior to adsorption of BDT. This information is necessary to determine the structures of adlayers. Adding BDT stock solution directly into the STM cell facilitated molecular adsorption. Depending on the concentration of BDT and the potential of Pt(111), it took seconds or hours to produce a full monolayer of BDT. In-situ STM imaging of Pt(111) at 0.15 V in 0.1 M $HClO_4$ yielded the results shown in Figure 2a and b, obtained 45 and 85 min after addition of BDT. Both images reveal long-range ordered structures punctuated by domain boundaries and packing defects.

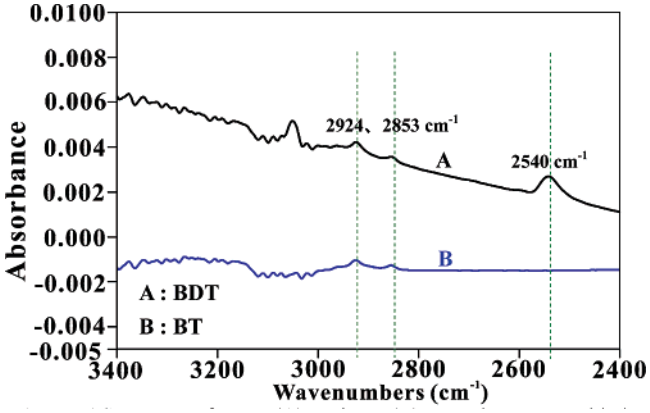

Figure 3. IRRAS spectra of BDT (A) and BT (B) monolayer assembled on Pt(111) surfaces.

The high-resolution STM images shown in Figure 2c and d discerned the arrangement of BDT on a terrain at different adsorption times. By referring to the atomic resolution of the Pt(111) substrate (not shown), it is possible to characterize unambiguously these two adlattices. Both arrays are hexagonal with nearest neighbor distances of 5.6 and 4.8 Å, respectively. Furthermore, protrusions are aligned along (Figure 2c) and rotated by 30° (Figure 2d) from the close-packed atomic rows of Pt(111). These results are indicative of (2×2) and $(\sqrt{3} \times \sqrt{3})R30°$ structures, respectively. The coverages of these adlattices are 0.25 and 0.33, respectively. Consequently, molecular adsorption continued with time to generate these two adlattices of BDT at different stages of adsorption. Because the intermolecular spacings of 4.8 and 5.6 Å of these two adlattices are larger than the van der Waals diameter of the benzene molecule, BDT and BT admolecules are likely adsorbed upright with their sulfur headgroups bonded directly to Pt(111). This tilt molecular orientation can have some bearing on the STM results, which show two sets of spots exhibiting unlike intensity. We attribute these features to the sulfur headgroups and phenyl end groups in the case of BT, respectively.[29] Similarly, the two sets of spots seen for the BDT adlattice (Figure 2d) can be explained. It is impossible to infer the position of the other sulfur headgroup in the adlayer from the present STM results. However, given the compactness of the adlattice, all admolecules would have to be aligned identically to minimize intermolecular repulsion.

IRRAS measurements were performed to probe the bonding configuration of BDT admolecules on Pt(111). Figure 3A and B shows the resultant IR spectra for BT and BDT, respectively. Both spectra contain two absorption bands at 2924 and 2853 cm^{-1} attributable to the C−H stretching of the benzene ring, while the band at 2540 cm^{-1} ascribable to the S−H stretching is seen for BDT only.[17−19,34,35] These results clearly indicate that both BT and BDT are bonded to Pt(111) via only one sulfur headgroup.

Electrodeposition of Au on BDT-Modified Pt(111) Electrode. The electrodeposition of Au onto BT- and BDT-modified Pt(111) was performed in 0.1 M $HClO_4$ + 0.01 mM $HAuCl_4$ under diffusion control. The potential of Pt(111) was held at

(33) Hamelin, A.; Martins, A. M. *J. Electroanal. Chem.* **1996**, *407*, 13−21.
(34) Pavia, D. L.; Lampman, G. M.; Kriz, G. S. *Introduction to Spectroscopy*; Harcourt College Publishers: Fort Worth, TX, 2001; p 79.
(35) Wan, L.-J.; Terashima, M.; Noda, H.; Osawa, M. *J. Phys. Chem. B* **2000**, *104*, 3563−3569.

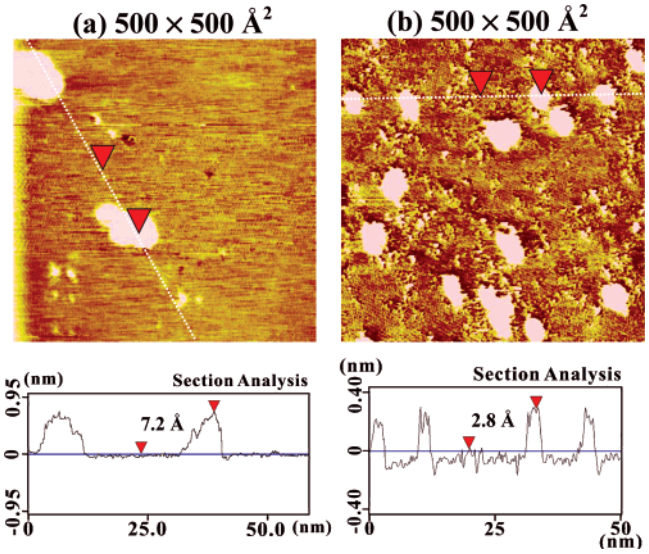

Figure 4. High-resolution STM images showing the gold clusters deposited on BT/Pt(111) (a) and BDT/Pt(111) (b). The section profiles along the dotted lines in a and b are shown below.

0.1 V prior to the addition of $HAuCl_4$. STM results (Figure 4) recorded at an early stage reveal gold nucleation on BT- and BDT-modified Pt(111). Gold deposit aggregated to form clusters distributed uniformly over the entire surface in both cases. The section analysis shown under the images reveals the heights of nucleation seeds on these Pt electrodes. The average height is 6.5−7 Å (3−4 atoms in height) on BT-modified Pt(111), as compared to 2.8 Å (monatomic) on BDT-modified Pt(111). Evidently, gold deposition proceeded in 3D and 2D manners on BT- and BDT-coated Pt(111) electrodes, respectively. Since BT and BDT were adsorbed as benzenethiolate, the only distinct difference between these cases is due to the presence of a pendant SH group of BDT but not of BT. We contend that this pendant SH group could interact specifically with the precursors of gold deposit and could slow the motion of Au adatoms on modified Pt(111). It has been shown that the deposit−substrate interaction and diffusion rate of adspecies are of the leading factors that dominate the growth mode of thin films; different growth modes were then expected under different conditions. The high density of smaller nucleation seeds of gold on BDT-modified Pt(111) supports the view of higher deposit−substrate interaction and slower diffusion rate of adspecies.

Subsequent gold deposition on BDT-coated Pt(111) is substantiated by the time-dependent STM images acquired at 0.15 V (Figure 5). Owing to the rather low concentration of $HAuCl_4$ (10 μM), gold was deposited at such a slow rate that in-situ STM could follow the whole process, from the initial nucleation (Figure 5a) to the final monolayer formation (Figure 5b−f). As demonstrated in Figure 5, gold adatoms nucleated randomly, followed by processes of diffusion, collapse, and aggregation into monatomic islands.

The 500 × 500 Å^2 scale (Figure 6a) reveals a pristine surface with only a few pits, attributed to the packing defects of the adlayer. Switching to a high-resolution imaging mode yielded molecular features on the gold-plated BDT/Pt(111) electrode. Figure 6b shows a 70 × 70 Å^2 STM scan which highlights an ordered array with a modulation in intensity. This structure is identified as Pt(111) − (6 × 2$\sqrt{13}$), which can be ascribed to Au adatoms or/and BDT admolecules. This moiré pattern is pseudo-hexagonal (Figure 6b), and the direction-dependent periodicities are 16.5, 17.8, and 22 Å as marked. A moiré pattern was noted in a previous study of gold deposition on Pt(111), but the modulation of intensity in that case is ca. 75 Å.[36] Mostly certainly this difference arises from the presence of BDT admolecules on Pt(111), which contrasts with the gold adlayer on a bare Pt(111) surface.

Deposition of Cu, Ag, and Pt on SAM-modified gold electrodes has been examined. The locations of metal deposit with respect to the thiol admolecules depend on the preference of thiol molecules to bind with, transport rate of thiol admolecules, and deposition rate of metal adatoms.[13,15,27] For example, Ag adatoms were found to go underneath the SAM layer of hexanethiol and deposited directly on gold electrode, whereas

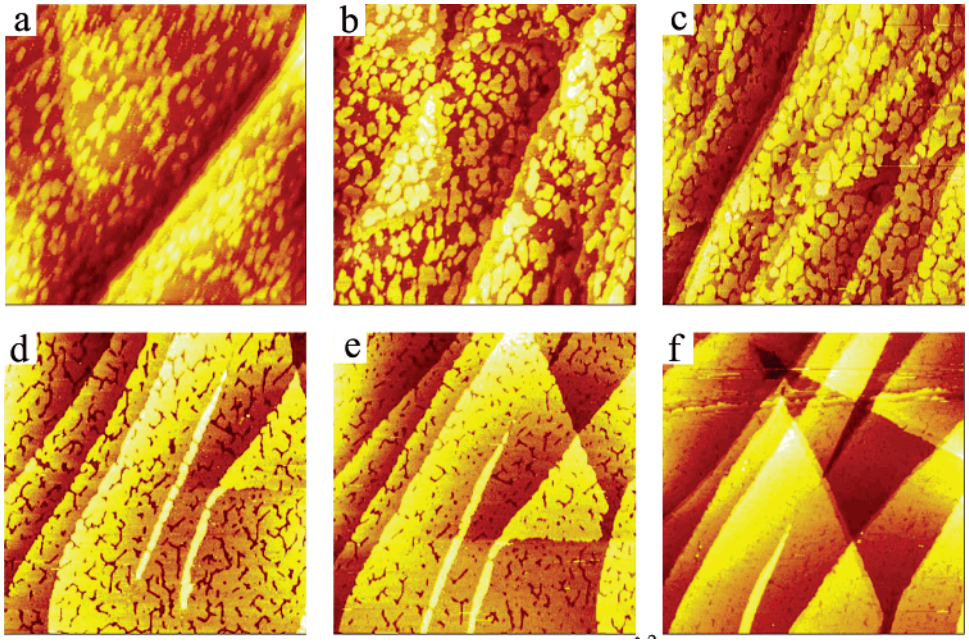

Figure 5. Time-sequenced STM images (3000 × 3000 Å^2) showing the deposition of gold on BDT/Pt(111) at 0.15 V.

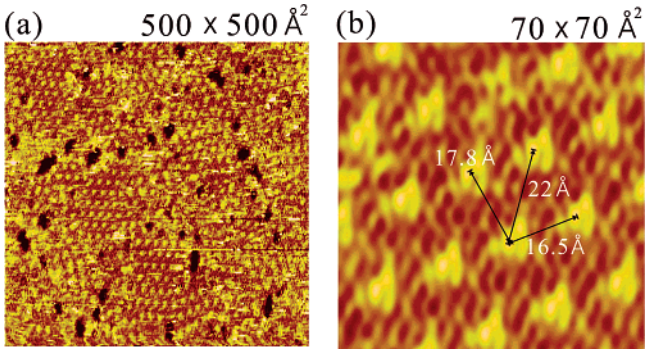

Figure 6. In-situ STM images obtained at a BDT/Pt(111) electrode after a monolayer of gold adatoms were deposited in 0.1 M $HClO_4$ + 0.01 mM $HAuCl_4$.

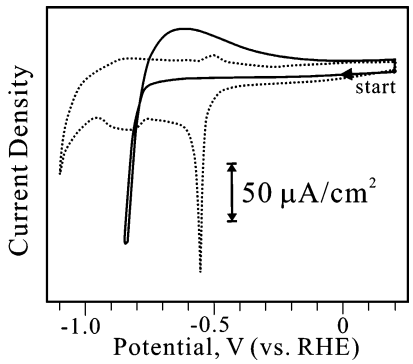

Figure 7. Cyclic voltammograms recorded at 50 mV/s for BDT-modified Au(111) (dotted trace) and gold-plated BDT/Pt(111) (solid trace) electrodes.

Cu adatoms are co-deposited with SAM adlayer.[17,18] In the present study, to resolve this issue, we conducted cyclic voltammetry on gold-plated, BDT-modified Pt(111) electrodes. The idea was to compare the stripping profiles obtained with gold-plated BDT/Pt(111) electrode and BDT/Au(111) in alkaline solutions. Since desorption of BDT from Au(111) results in a well-defined reduction peak, whether the same result is observed for a gold-deposited BDT/Pt(111) electrode would help to resolve the issue concerning the location of Au adatoms on the BDT/Pt(111) electrode. Figure 7 shows the CVs of gold-deposited BDT/Pt(111) and BDT/Au(111) electrodes (solid and dotted traces, respectively) recorded at 50 mV/s in 1 M KOH. Reductive desorption of BDT from the Au(111) electrode produced a reduction peak at −0.55 V (RHE) in the negative-going potential sweep from 0.2 to −1.1 V, as noted for BT[35] and 4-pyridinethiol[37] adsorbed on Au(111). In contrast, the negative potential sweep from 0.2 to −0.8 V (the onset of water reduction) for BDT/Pt(111) (not shown here) and gold-plated BDT/Pt(111) (Figure 7) electrodes did not result in this feature, suggesting BDT was strongly held on Pt(111) before and after gold deposition. Gold adatoms overlaid the BDT adlayer rather than displaced it. This result is anticipated because BDT was held more firmly on Pt(111) than on Au(111).

In comparison, we examined the subsequent gold deposition on BT-modified Pt(111) under the same experimental conditions. The resultant time-dependent STM images are shown in Figure 8. Gold adatoms were deposited into 3D islands distributed uniformly over the entire surface at an early stage. As described earlier, these islands are 3−4 atomic layers in height and grew laterally and vertically with time. Regardless of the length of deposition time, this 3D growth mode predominated to produce a rough Pt(111) surface revealed by the STM. The contrast between the results in Figures 5 and 8 is so distinct that the effect of organic modifiers on metal deposition is beyond doubt.

Conclusion

In-situ STM was used to study the structures of a BDT adlayer on Pt(111) electrode and electrodeposition of gold on BDT- and BT-modified Pt(111) electrodes. BDT admolecules were first adsorbed in Pt(111) − (2 × 2) structure and then transformed into $(\sqrt{3} \times \sqrt{3})R30°$ structure later. The high-resolution STM image and IRRAS measurement reveal that BDT molecule was attached to the Pt(111) electrode with one sulfur headgroup, while the other SH group was pendant on the surface. The latter could strongly interact with the deposited

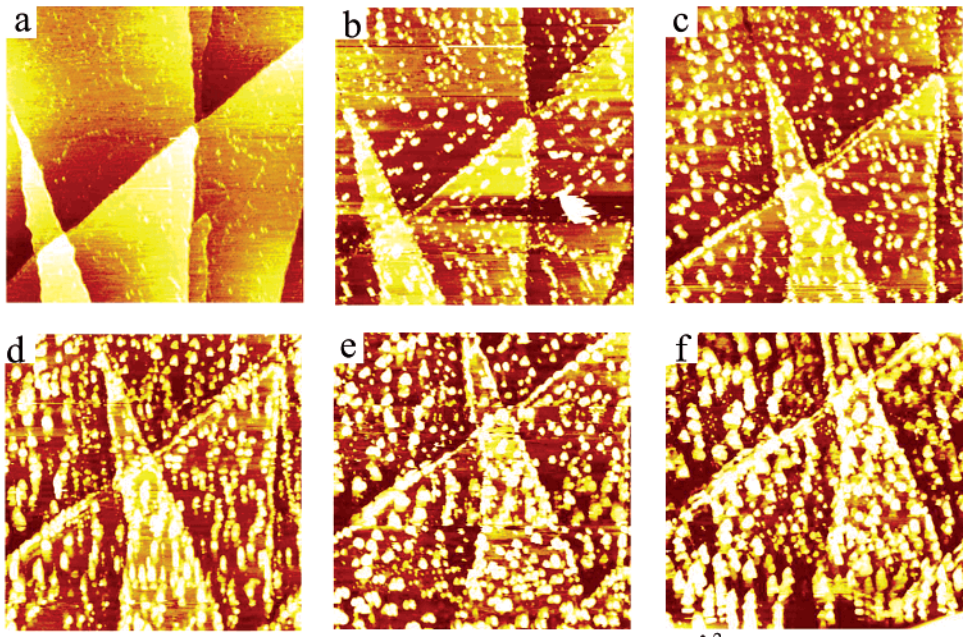

Figure 8. Time-sequenced STM images (3000 × 3000 Å²) showing the slow deposition of gold on BT/Pt(111) at 0.15 V in 0.1 M $HClO_4$ + 0.01 mM $HAuCl_4$.

gold adatoms and slow the diffusion rate of gold adatoms. These characteristics afford a 2D layered-type growth mode. Stripping voltammetric analysis indicates that gold adatoms are co-deposited with the BDT adlayer rather than inserted between BDT and Pt substrate. In contrast, gold adatoms were deposited into 3D islands on the BT/Pt(111) electrode from the initial nucleation stage to the growth of a thicker film. This study illustrates unambiguously that an organic surface modifier can influence greatly how smooth a metallic film can be produced.

(36) Sibert, E.; Ozanam, F.; Maroun, F.; Behm, R. J.; Magnussen, O. M. *Surf. Sci.* **2004**, *572*, 115−125.
(37) Yoshimoto, S.; Yoshida, M.; Kobayashi, S.; Nozute, S.; Miyawaki, T.; Hashimoto, Y.; Taniguchi, I. *J. Electroanal. Chem.* **1999**, *473*, 85−92.

Acknowledgment. The partial support of this research by the National Science Council of Taiwan through grant number NSC 94-2214-E-006-022 and NSC 93-2120-M-006-007 is gratefully acknowledged.

JA0569407